Chemistry and Physics of Lipids 221 (2019) 30–38

Contents lists available at ScienceDirect

Chemistry and Physics of Lipids

journal homepage: www.elsevier.com/locate/chemphyslip

Influence of Mg^{2+} and Ca^{2+} on nanodisc formation by diisobutylene/maleic acid (DIBMA) copolymer

Bartholomäus Danielczak[a], Annette Meister[b], Sandro Keller[a,*]

[a] Molecular Biophysics, Technische Universität Kaiserslautern (TUK), Erwin-Schrödinger-Str. 13, 67663 Kaiserslautern, Germany
[b] ZIK HALOmem, Martin Luther University Halle–Wittenberg, Kurt-Mothes-Str. 3a, 06120 Halle (Saale), Germany

ARTICLE INFO

Keywords:
Divalent cations
Polymer nanodiscs
Coulombic repulsion
Lipid exchange
Membrane solubilization

ABSTRACT

Most membrane-solubilising amphiphilic copolymers such as diisobutylene/maleic acid (DIBMA) and styrene/maleic acid (SMA) carry high negative charge densities. Their polyanionic character results in strong Coulombic repulsion, both between polymer chains and lipid membranes during the solubilisation process as well as among polymer-encapsulated nanodiscs after solubilisation. Coulombic repulsion is attenuated by charge screening and, more efficiently, by counterion association, which is particularly strong for multivalent cations binding to polyanionic copolymers. Here, we investigated the effects of the two common alkaline earth metal ions Mg^{2+} and Ca^{2+} on the solubilisation properties of and the nanodiscs formed by DIBMA. By quantifying the kinetics and the equilibrium efficiency of lipid solubilisation by static and dynamic light scattering, respectively, we found that millimolar concentrations of Mg^{2+} or Ca^{2+} accelerated DIBMA-mediated lipid solubilisation several-fold and resulted in considerably smaller nanodiscs than without divalent cations. Time-resolved Förster resonance energy transfer spectroscopy revealed that collisional transfer of phospholipids among nanodiscs was up to ~20 and ~25 times faster in the presence of 10 mM Mg^{2+} or 7.5 mM Ca^{2+} than in the absence of divalent cations. These major effects of Mg^{2+} and Ca^{2+} contrasted with a moderate influence on the morphology and the thermotropic phase behaviour of the nanodiscs. Finally, we compared the yields of membrane-protein extraction from *Escherichia coli* membranes, which increased by up to two-fold upon addition of Mg^{2+} or Ca^{2+}. None of these effects could be explained by Coulombic screening alone, as the change in ionic strength resulting from low millimolar concentrations of divalent cations was minor. Thus, we conclude that Mg^{2+} and Ca^{2+} specifically associated with DIBMA to neutralise part of the polymer's carboxylate groups.

1. Introduction

Nanodiscs encapsulated by amphiphilic copolymers such as diisobutylene/maleic acid (DIBMA) (Oluwole et al., 2017a,b), styrene/maleic acid (SMA) (Tonge and Tighe, 2001; Knowles et al., 2009), and styrene/maleimide (SMI) (Hall et al., 2018) have attracted great attention because they form spontaneously upon addition of these polymers to cellular or model membranes, thereby extracting membrane proteins and surrounding lipids. Membrane proteins embedded in such lipid-bilayer nanodiscs are often more stable and functional than in detergent micelles (Jamshad et al., 2015; Barniol-Xicota and Verhelst, 2018) and are amenable to a wide range of biophysical techniques (Orwick-Rydmark et al., 2012; Dörr et al., 2014; Oluwole et al., 2017a), structural methods (Bersch et al., 2017; Broecker et al., 2017; Parmar et al., 2017; Sun et al., 2018), and activity assays (Gulati et al., 2014; Jamshad et al., 2015; Logez et al., 2016; Oluwole et al., 2017a; Damian et al., 2018; Barniol-Xicota and Verhelst, 2018).

DIBMA and various SMA variants, which currently are the most widely used copolymers, contain large fractions of maleic acid residues, ranging from 25 mol% for SMA(3:1) up to 50 mol% for DIBMA. Hence, these highly anionic copolymers experience strong Coulombic repulsion, which acts both between membrane-adsorbed and free polymer chains during the solubilisation process as well as among nanodiscs once the latter have formed. In general, Coulombic repulsion can be reduced by two nonexclusive mechanisms: (i) Coulombic screening resulting from an increase in the ionic strength of the aqueous solution is independent of the chemical nature of the screening ions and, thus, depends only on their concentrations and charge numbers (Bergethon, 2010). (ii) Association of counterions with charged groups on the polymer, by contrast, additionally depends on the chemical properties of the associating counterions (Moelwyn-Hughes, 1963).

Coulombic screening due to an increase in the ionic strength of the

* Corresponding author.
E-mail address: mail@sandrokeller.com (S. Keller).

https://doi.org/10.1016/j.chemphyslip.2019.03.004
Received 18 November 2018; Received in revised form 8 March 2019; Accepted 11 March 2019
Available online 13 March 2019
0009-3084/

solution strongly influences the formation and the dynamics of SMA- and DIBMA-bounded nanodiscs. For instance, increasing the concentration of NaCl accelerates nanodisc formation by SMA(2:1) (Scheidelaar et al., 2015, 2016), enhances the solubilisation efficiency by DIBMA (Oluwole et al., 2017b), speeds up collisional lipid transfer among nanodiscs bounded by SMA(2:1) (Grethen et al., 2018) or DIBMA (Danielczak and Keller, 2018), and increases the yield of membrane-protein extraction by SMA(2:1) (Dörr, 2017). All of these effects are ascribed primarily to Coulombic screening because the association of Na^+ and other monovalent ions with carboxylate groups is relatively weak (Kläning and Østerby, 1976; Ederth, 2000). By contrast, divalent cations are expected to attenuate Coulombic repulsion even more efficiently than monovalent ions do because, in addition to raising the ionic strength, they associate much more strongly with polyanionic polymers (Bretti et al., 2005). However, the influence of divalent cations on the formation and the properties of polymer-encapsulated nanodiscs have not been investigated thus far. The prime reason for this might be that nanodiscs made from SMA(3:1) or SMA(2:1) precipitate in the presence of even low millimolar concentrations of Mg^{2+} or Ca^{2+} (Oluwole et al., 2017a; Hall et al., 2018). By contrast, DIBMA-bounded nanodiscs are stable up to 25 mM Mg^{2+} or 20 mM of Ca^{2+} (Oluwole et al., 2017a), thus offering a sufficiently wide window for testing the role of these divalent cations.

By employing static and dynamic light scattering (SLS and DLS, respectively), time-resolved Förster resonance energy transfer (TR-FRET) spectroscopy, and quantitative sodium dodecyl sulphate polyacrylamide gel electrophoresis (SDS-PAGE), we found that low millimolar concentrations of Mg^{2+} or Ca^{2+} substantially increased the kinetics and equilibrium efficiency of DIBMA-mediated lipid solubilisation, accelerated lipid transfer among DIBMA/lipid particles (DIBMALPs), and promoted membrane-protein extraction from cellular membranes upon incubation with DIBMA. Crucially, transmission electron microscopy (TEM) and differential scanning calorimetry (DSC) confirmed that both the overall nanodisc morphology as well as the lipid-bilayer architecture were retained at elevated concentrations of divalent cations.

2. Experimental section

If not stated otherwise, all experiments were performed using 50 mM Tris, 200 mM NaCl, pH 7.4 with the indicated concentrations of $MgCl_2$ or $CaCl_2$.

2.1. Materials

DIBMA (Sokalan CP 9, M_n = 8.4 kg mol^{-1}, M_w = 15.3 kg mol^{-1}) was a kind gift from BASF (Ludwigshafen, Germany). 1,2-dimyristoyl-*sn*-glycero-3-phosphocholine (DMPC) and 1-palmitoyl-2-oleoyl-*sn*-glycero-3-phosphocholine (POPC) were kindly provided by Lipoid (Ludwigshafen, Germany). *N*-(7-nitrobenz-2-oxa-1,3-diazol-4-yl)-1,2-dihexadecanoyl-*sn*-glycero-3-phosphoethanolamine (NBD-PE) and *N*-(lissamine rhodamine B sulphonyl)-1,2-dihexadecanoyl-*sn*-glycero-3-phosphoethanolamine (Rh-PE) were purchased from Fisher Scientific (Schwerte, Germany) and Biotium (Fremont, USA), respectively. Tris (hydroxymethyl)aminomethane (Tris) was from Carl Roth (Karlsruhe, Germany) and NaOH from Sigma–Aldrich (Steinheim, Germany). NaCl and CH_3OH were from VWR (Darmstadt, Germany), and $CHCl_3$ was from Fisher Scientific. All chemicals were purchased in the highest purity available.

2.2. Preparation of DIBMA stock solution

We placed 2.5 mL of a commercial DIBMA solution into a 5-mL QuixSep microdialysis capsule (Carl Roth) and dialysed this solution using a Spectra/Por 3 dialysis membrane (Spectrum Laboratories, Rancho Dominguez, USA) with a nominal molar-mass cutoff ; of 3.5 kg mol^{-1}. Dialysis was performed at room temperature against 1 L of buffer for 24 h with buffer exchange after 16 h. Then, the DIBMA stock solution was sterile-filtered through a syringe filter (Carl Roth) with a nominal pore diameter of 220 nm. We determined DIBMA concentrations by refractometry on an Abbemat 500 (Anton Paar, Graz, Austria) using dn/dc = 1.346 M^{-1} based on M_n (Oluwole et al., 2017a).

2.3. Preparation of large unilamellar vesicles (LUVs)

DMPC or POPC powder was suspended in buffer to a final lipid concentration of 50 mM. We vortexed these lipid suspensions for 2 min prior to 31-fold extrusion through two stacked polycarbonate membranes with a nominal pore diameter of 100 nm. DMPC was extruded at 35 °C using a block-heated Mini-Extruder (Avanti, Alabama, USA) and POPC at room temperature using a LiposoFast extruder (Avestin, Ottawa, Canada). DLS (see below) confirmed unimodal particle size distributions, yielding hydrodynamic LUV diameters of ~140 nm for DMPC and ~160 nm for POPC.

2.4. Solubilisation kinetics and efficiency

To assess the kinetics of lipid solubilisation, time-resolved SLS experiments were carried out on an SF.3 stopped-flow apparatus (Applied Photophysics, Leatherhead, UK) equipped with a (470 ± 10) nm light-emitting diode, whose output was set to 20 mA, and a photomultiplier mounted at a right angle. Drive syringes, tubes, and the quartz glass cell were thermostatted at 25 °C for POPC or 30 °C for DMPC. Samples were equilibrated for at least 10 min prior to each measurement. Then, 75-µL aliquots of POPC or DMPC LUVs at a lipid concentration of 5 mM were mixed rapidly with equal volumes of 2.5 mM or 0.5 mM DIBMA for POPC or DMPC, respectively, in buffer without divalent cations or with 5, 10, 15, or 20 mM $MgCl_2$ or $CaCl_2$. Temporal changes in scattering intensity were recorded 5 times with 10'000 data points for the first 10 s followed by 6000 data points for 1200 s or 40 s for POPC or DMPC, respectively. Scattering transients thus obtained were averaged. As a simple and robust metric, the time constant of solubilisation, τ, was taken as the time after mixing at which the scattering intensity, $I_{90°}$, reached a value of 4.5 (cf. Fig. 1a,b,d,f below). Divalent cation salts were added to the DIBMA solution prior to solubilisation; results were identical when these salts were added to the LUV suspension instead (data not shown).

In order to evaluate the equilibrium efficiency of lipid solubilisation, POPC LUVs were mixed with DIBMA and divalent cations to yield final concentrations of 5 mM POPC, 0–3.3 mM DIBMA, and 0, 3.3, 6.7, or 10.0 mM $MgCl_2$ or 0, 2.5, 5.0, 7.5, or 10 mM $CaCl_2$. Samples were incubated for 1 h at 35 °C under vigorous shaking, followed by 15 h of incubation at 37 °C. Particle size distributions were monitored by DLS at 25 °C (see below).

2.5. Preparation of DIBMALPs for TR-FRET

Fluorescently labelled DIBMALPs were produced by separately dissolving powders of DMPC, NBD-PE, and Rh-PE in $CHCl_3$ before mixing them at a molar ratio of 99.3:0.3:0.3. We obtained a thin lipid film after solvent removal using a Rotavapor R-210 evaporator (Büchi, Essen, Germany). Solvent traces were removed under high vacuum in a desiccator for at least 16 h. We suspended the lipid films in buffer by vortexing at 35 °C before performing at least six freeze–thaw cycles. We then solubilised suspensions having a final lipid concentration of 5 mM using 0.5 mM DIBMA at 35 °C with gentle agitation for ~16 h and subsequently centrifuged for 5 min at 20,000 *g*. For unlabelled DIBMALPs, we used the same lipid/polymer ratios at a total lipid concentration of 10 mM. For both labelled and unlabelled DIBMALPs, unimodal nanodisc size distributions were confirmed by DLS (see below), yielding *z*-average hydrodynamic diameters of $d_z \approx$ 30 nm. Inclusion of 0.3 mol% of each of the two fluorescently labelled lipids

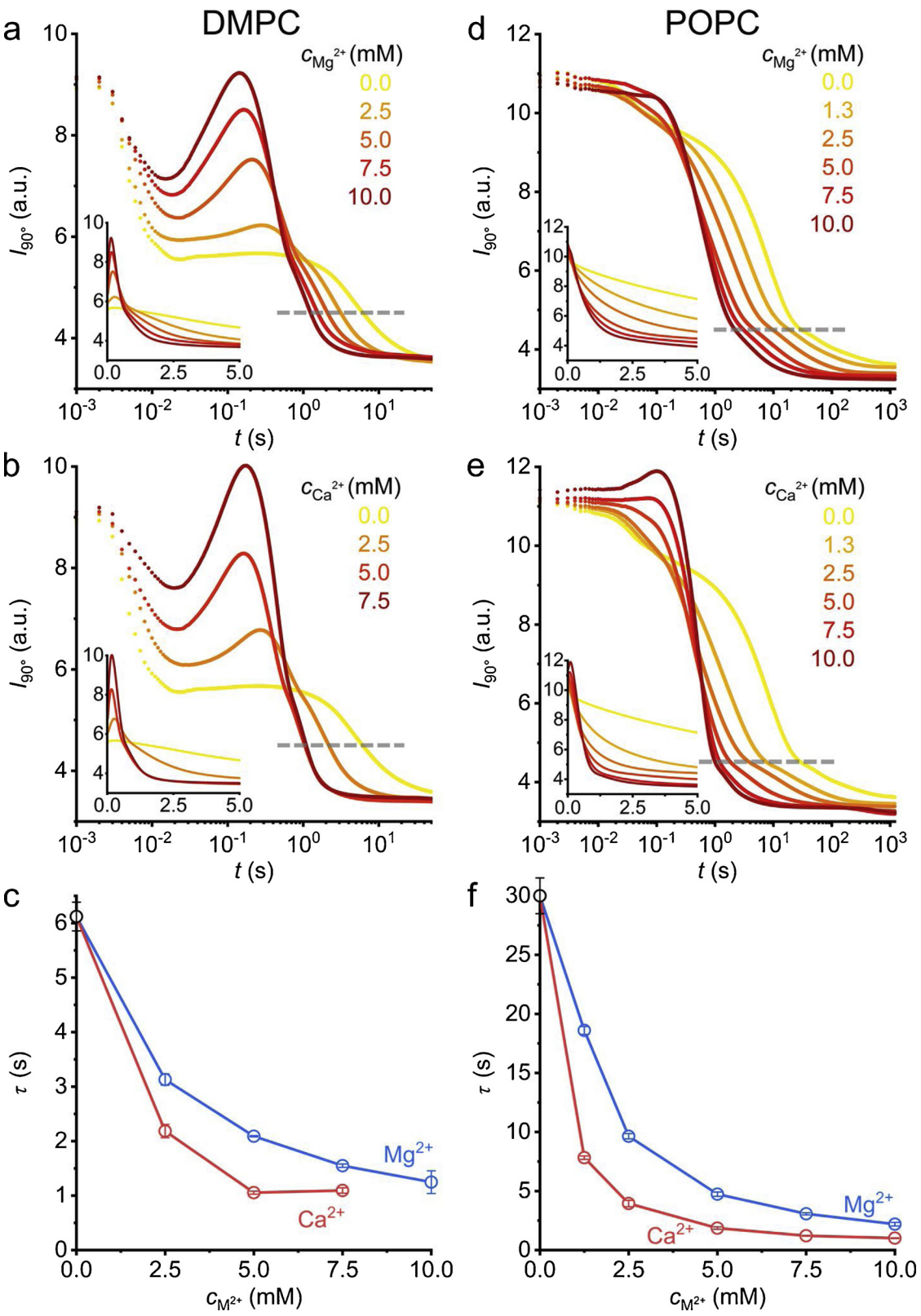

Fig. 1. Solubilisation kinetics of (a–c) DMPC and (d–f) POPC LUVs by DIBMA at 30 °C and 25 °C, respectively, in the presence of increasing concentrations of divalent cations, $c_M{}^{2+}$, as followed by stopped-flow SLS. (a,b,d,e) Scattering intensities at 90°, $I_{90°}$, as functions of time, t, after mixing DMPC LUVs or POPC LUVs and DIBMA to yield final lipid and polymer concentrations of, respectively, 2.5 mM lipid and 0.25 mM or 1.25 mM DIBMA in the presence of various concentrations of (a,d) Mg^{2+} or (b,e) Ca^{2+}. Insets show the same data on linear time axes. Grey horizontal lines denote the threshold at $I = 4.5$ used to define time constants of solubilisation. (c,f) Time constants, τ, derived from data in panels a, b, d, and e in dependence on $c_M{}^{2+}$. Error bars (within circles) represent standard deviations of 5 stopped-flow experiments.

had no effect on particle size distributions as compared with those of DIBMALPs containing only DMPC, as also found earlier for 1 mol% of each (Cuevas Arenas et al., 2017; Grethen et al., 2018; Danielczak and Keller, 2018). Addition of divalent cations up to 10 mM at a DIBMA/DMPC molar ratio of 0.1 had no significant effect on particle size distributions (data not shown).

2.6. TR-FRET

Time-dependent donor dequenching was measured on an SF.3 stopped-flow apparatus equipped with a (470 ± 10) nm light-emitting diode, whose output was set to 10–20 mA and further attenuated by an OD 2 filter to avoid photobleaching. Fluorescence emission was blocked below 513 nm and above 543 nm with a TechSpec OD 6 band-pass filter (Edmund Optics, Karlsruhe, Germany) and was monitored with a photomultiplier mounted at a right angle. Drive syringes, tubes, and the quartz glass cell were thermostatted at 30 °C at all times. Samples were equilibrated for at least 10 min prior to each measurement. Then, 75-µL aliquots of fluorescently labelled DIBMALPs at a lipid concentration of 5 mM were mixed rapidly with equal volumes of unlabelled DIBMALPs at a lipid concentration of 10 mM. Time-dependent emission from NBD-PE was recorded 6–7 times with 10'000 data points per shot. The fluorescence transients thus obtained were averaged and analysed by nonlinear least-squares fitting (Kemmer and Keller, 2010). Provided that lipid exchange takes place, mixing labelled and unlabelled DIBMALPs leads to a redistribution and dilution of NBD-PE and Rh-PE. This process increases the average distance between the fluorophores and thus reduces donor quenching. Consequently, the fluorescence emission intensity of NBD-PE at 530 nm increases exponentially:

$$F(t) = F_\infty + e^{-k_{obs}t}(F_0 - F_\infty) \quad (1)$$

Here, $F(t)$ is the intensity at time t after mixing, k_{obs} is the observed rate constant, and F_0 and F_∞ are the initial and final fluorescence emission intensities, respectively. At the rather high lipid concentrations used in this study, lipid exchange occurs predominantly by binary collisions between two nanodiscs (Danielczak and Keller, 2018). Thus, we could approximate the second-order rate constant characterising the kinetics of lipid exchange through binary collisions, k_{bi}, by dividing the observed rate constant, k_{obs}, by the lipid concentration in unlabelled nanodiscs (cf. text).

2.7. Electrostatic calculations

We used simple electrostatic theory to estimate the effect of Coulombic screening on k_{bi} as it would manifest in the absence of counterion association with the polymer. To this end, we relied on an extended version of the Debye–Hückel equation (Bergethon, 2010), which we have found suitable for DIBMALPs (Danielczak and Keller, 2018). Here, this equation was rearranged to read:

$$\log \frac{k_{bi}^{M^{2+}}}{k_{bi}^{w/o}} = 2Az^2\left(\frac{\sqrt{I_{M^{2+}}}}{1 + Br\sqrt{I_{M^{2+}}}} - \frac{\sqrt{I_0}}{1 + Br\sqrt{I_0}}\right) \quad (2)$$

where $k_{bi}^{M^{2+}}$ and $k_{bi}^{w/o}$ are the second-order rate constants characterising lipid exchange through binary collisions with and without divalent cations. r and z are the radius and the effective charge number of DIBMALPs under the assumption that there is no counterion association, respectively, $I_{M^{2+}}$ and I_0 are the ionic strengths in the presence and absence of divalent cations, respectively, and A and B are constants (Bergethon, 2010). Since we have previously obtained $z = -47$ for $r = 11.5$ nm (Danielczak and Keller, 2018), we used these values for computing $k_{bi}^{M^{2+}}$ from $k_{bi}^{w/o}$. Note, however, that the DIBMALPs used here were larger and had a lower charge density, and, thus, a lower effective charge number. Therefore, our estimate provides an upper limit because, according to Eq. (2), both larger r and smaller z would result in a lower $k_{bi}^{M^{2+}}$ value.

2.8. Dynamic light scattering

DLS measurements were performed on a Zetasizer Nano S90 (Malvern Instruments, Malvern, UK) working with a 633-nm He–Ne laser and a detection angle of 90°. Samples were thermostatted for 2 min at 30 °C for DMPC or 25 °C for POPC before measurements were performed in a 45-µL quartz glass cuvette having a cross-section of 3 mm × 3 mm (Hellma Analytics, Müllheim, Germany). For determination of particle size distributions, the instrument software was allowed to automatically optimise the attenuator settings. During data analysis, we accounted for the influence of all buffer components and, in particular, of different concentrations of divalent cations on the viscosity and refractive index of the solvent. Autocorrelation functions were fitted using a non-negatively constrained least-squares function (Hassan et al., 2015) to yield intensity-weighted particle size distributions and by cumulant analysis (Koppel, 1972) to obtain d_z values and associated polydispersity indices (PDIs). Distribution widths of d_z, σ, were calculated as $\sigma = \sqrt{PDI}\, d_z$.

2.9. TEM

Samples were prepared by incubating 5 µL of a buffered solution containing 1 mM POPC, 0.5 mM DIBMA, and 10 mM $MgCl_2$ or $CaCl_2$ on an SF162 Cu grid coated with Formvar film (Plano, Wetzlar, Germany). After 60 s, excess liquid was blotted off with filter paper, and grids were washed twice with buffer. This was immediately followed by staining with 5 µL of a 1% (*w/v*) aqueous uranyl acetate solution, which was blotted off after 30 s. Grids were examined on an EM 900 transmission electron microscope (Carl Zeiss, Oberkochen, Germany), and micrographs were taken with a BM-2k-120 dual-speed on axis slow-scan charge-coupled device (SSCCD) camera (TRS, Moorenweis, Germany).

2.10. DSC

Samples containing 5 mM DMPC and 0.5 mM DIBMA in buffer and either 10 mM Mg^{2+}, 7.5 mM Ca^{2+}, or no divalent cations were incubated at 30 °C for 16 h. Formation of nanodiscs was confirmed by DLS, which confirmed particle diameters of $d_z \approx$ 23 nm. Buffer-filled sample and reference cells were repeatedly heated and cooled at a rate of 30 °C h^{-1} before the buffer in the sample cell was replaced with sample. Apart from the first upscan, successive heating and cooling scans overlaid very closely. Data were blank-subtracted and normalised against the DMPC concentration using the software MicroCal Origin 7.0 (OriginLab, Northampton, USA). The main gel-to-fluid transition temperature, T_m, was taken as the temperature at which the excess molar isobaric heat capacity, ΔC_p, reached a maximum.

2.11. Extraction of membrane proteins from E. coli membranes

We transformed *E. coli* BL21(DE3) cells with an empty pET-24 vector and selected by kanamycin resistance. After incubation in M9 minimal medium overnight at 37 °C under permanent agitation, cells were harvested by centrifugation at 4000 *g* and washed with saline (154 mM NaCl). Cell pellets were resuspended in a 10-fold volume of ice-cold 100 mM Na_2CO_3 and ultrasonicated twice for 10 min in an S-250A sonifier (Branson Ultrasonics, Danbury, USA). Cell debris and unbroken cells were removed by centrifugation at 3000 *g* and 4 °C for 20 min. The supernatant was ultracentrifuged for 1 h at 100,000 *g* and 4 °C and washed with buffer (50 mM Tris, 200 mM NaCl, 2 mM EDTA, pH 7.4). Membrane pellets were resuspended in buffer (50 mM Tris, 200 mM NaCl, 0.5 mM EDTA, pH 7.4) to a final concentration of 25 mg mL^{-1} wet mass and treated with 3.0 mM (i.e., 2.5% (*w/v*)) DIBMA and 10.5 mM $MgCl_2$, 8.0 mM $CaCl_2$, or buffer without divalent cations. Samples were incubated at 25 °C with gentle agitation and subjected to ultracentrifugation for 50 min at 100,000 *g* and 15 °C. Aliquots were taken after 0.2, 1, 2, 4, 7, and 23 h of incubation. As a

control, a sample without DIBMA and without divalent cations was treated identically and was ultracentrifuged after 23 h before the supernatant was analysed by SDS-PAGE. To avoid band smearing caused by the presence of polymers (Lee et al., 2016), we precipitated the solubilised fractions with $CH_3OH/CHCl_3/H_2O$ in a mixing ratio of 4:1:3 (*v/v/v*) (Wessel and Flügge, 1984). Briefly, to a 200-µL aliquot of ice-cold sample, we successively added 800 µL ice-cold CH_3OH, 200 µL ice-cold $CHCl_3$, and 600 µL ice-cold water with thorough vortexing after each addition. The mixture was centrifuged for 5 min at 14,000 *g* and 1 °C. The upper, aqueous layer was removed, and 800 µL CH_3OH was added before the sample was vortexed again. Precipitated proteins were pelleted by centrifugation for 1 min at 5000 *g* and another 5 min at 20,000 *g*, both at 1 °C. Without disturbing the pellet, we carefully removed CH_3OH using a pipette. Residual organic solvent was allowed to evaporate for 1 h at 37 °C. The dried pellet was resuspended in 50 µL SDS buffer (106 mM Tris-HCl, 141 mM Tris, 2% (*w/v*) SDS, 10% (*w/v*) glycerol, 0.51 mM EDTA, 0.22 mM Coomassie Brilliant Blue G250, 0.175 mM Phenol Red, pH 8.5), boiled for 10 min under rocking agitation, and subjected to SDS-PAGE. Protein extraction yields were quantified by densitometry using the public-domain software ImageJ (Schneider et al., 2012), and data were corrected by subtracting control (i.e., buffer-only) and background levels.

3. Results and discussion

3.1. Kinetic and equilibrium efficiencies of lipid solubilisation

To assess the influence of divalent cations on the kinetics of lipid solubilisation, we exploited time-resolved SLS to follow the disintegration of LUVs composed of the fully saturated phospholipid DMPC or the monounsaturated phospholipid POPC upon addition of DIBMA in the presence of increasing concentrations of Mg^{2+} and Ca^{2+} (Fig. 1). Upon mixing LUVs and DIBMA in a stopped-flow apparatus, we observed an initial decrease, a transient increase for DMPC or a plateau for POPC, and finally a massive drop in the intensity of scattered light, all of which became faster and more pronounced with increasing concentrations of Mg^{2+} (Fig. 1a,d) or Ca^{2+} (Fig. 1b,e). To quantify the kinetics of vesicle solubilisation, we defined the time constant of solubilisation, τ, as the time point at which the scattering intensity, I, reached a value of 4.5 (Fig. 1a,b,d,e, grey horizontal bars). For DMPC, τ decreased monotonically from (6.1 ± 0.3) s in the absence of divalent cations to (1.2 ± 0.2) s or (1.1 ± 0.1) s in the presence of 10 mM Mg^{2+} or 7.5 mM Ca^{2+}, respectively (Fig. 1c). As compared with DMPC, POPC solubilisation was ~5-fold slower in the absence of divalent cations, as reflected in a τ value of (30.0 ± 1.5) s, but became similarly fast upon addition of 10 mM Mg^{2+} or Ca^{2+}, with τ values of (2.2 ± 0.2) s and (1.0 ± 0.02) s, respectively. The transient increase or plateau in light scattering intensity that commenced ~10 ms after mixing most likely resulted from noncovalent vesicle crosslinking by polymer chains, as we have previously observed under equilibrium conditions for subsolubilising concentrations of DIBMA (Oluwole et al., 2017a, b). This interpretation was supported by the observation that the transient increase or plateau was more pronounced and shifted to earlier times with increasing $c_M{}^{2+}$, which is expected to accelerate and intensify interactions among highly negatively charged vesicles or vesicle fragments.

To evaluate the effects of divalent cations on the equilibrium efficiency of vesicle solubilisation, we focussed on POPC for which the kinetic effects of divalent cations were much more drastic. To this end, we monitored particle size distributions with the aid of DLS as functions of the polymer/lipid ratio (Fig. 2a,b). The availability of DIBMA/POPC pseudo-phase diagrams derived from ^{31}P-NMR spectroscopy (Oluwole et al., 2017b) allowed for a straightforward interpretation of the present DLS data. Increasing Mg^{2+} or Ca^{2+} concentrations reduced the amount of DIBMA required for complete solubilisation and, at each given DIBMA/POPC ratio, gave rise to particles that were consistently smaller

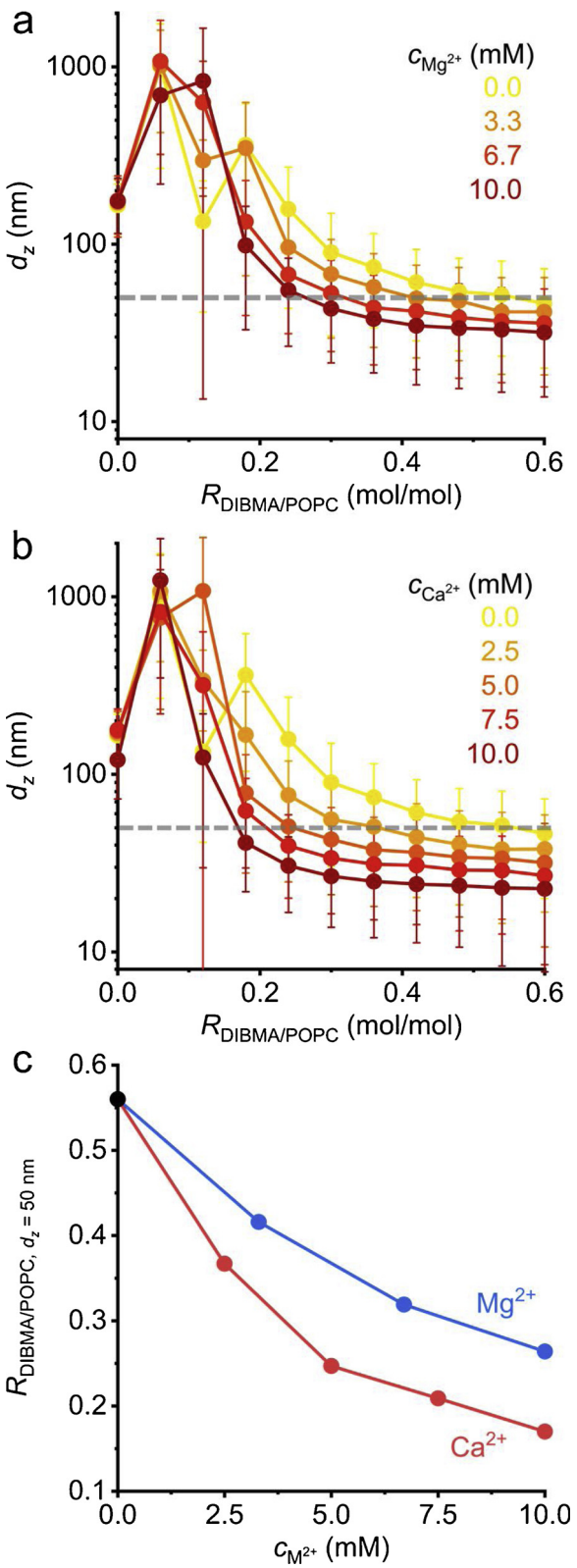

Fig. 2. Solubilisation efficiency of POPC LUVs by DIBMA at 25 °C and increasing $c_M{}^{2+}$ as monitored by DLS. (a,b) *z*-Average particle diameters, d_z, of 5 mM POPC as functions of DIBMA/POPC molar ratio, $R_{DIBMA/POPC}$, in the presence of various concentrations of (a) Mg^{2+} or (b) Ca^{2+}. Error bars reflect widths of particle size distributions as given by $\sigma = \sqrt{PDI}\, d_z$. Grey horizontal lines denote the threshold at d_z = 50 nm used for further quantification of equilibrium solubilisation efficiencies. (c) DIBMA/POPC molar ratios at which particles reached d_z = 50 nm as derived from data in panels a and b.

than without divalent cations. As an example, formation of 50-nm particles (Fig. 2a,b, grey horizontal lines) would require a DIBMA/POPC molar ratio of 0.56 in the absence of divalent cations, which contrasts with ratios of only 0.26 and 0.17 in the presence of 10 mM Mg^{2+} or Ca^{2+}, respectively (Fig. 2c). At the highest DIBMA/POPC molar ratio tested, *z*-average diameters and associated size distribution widths were (32 ± 18) nm and (23 ± 15) nm in the presence of 10 mM Mg^{2+} and Ca^{2+}, respectively, as compared with (46 ± 26) nm in the absence of divalent cations. For comparison, a much higher concentration of 200 mM NaCl is required to bring about a similar reduction in DIBMALP size under otherwise similar conditions (Oluwole et al., 2017b).

In conclusion, the above time-resolved and equilibrium solubilisation experiments showed that the formation of DIBMALPs became substantially faster and thermodynamically more efficient with increasing concentrations of divalent cations. The finding that Ca^{2+} had a more pronounced influence than Mg^{2+} indicated that these effects were not exclusively due to enhanced Coulombic screening at elevated ionic strength, as will be discussed in more detail below.

3.2. Kinetics of lipid exchange among DIBMALPs

To scrutinise the impact of divalent cations on the kinetics of lipid exchange among DIBMALPs, we used a time-resolved fluorescence dequenching assay (Nichols and Pagano, 1983). For this purpose, we produced fluorescently labelled DIBMALPs consisting of a DMPC matrix hosting 0.3 mol% of each NBD-PE and Rh-PE as donor and acceptor fluorophores, respectively. When co-localised within the same nanodisc, NBD-PE and Rh-PE form an efficient FRET pair, but redistribution of fluorescent lipids upon mixing with unlabelled nanodiscs in a stopped-flow apparatus will dequench the donor, thus resulting in an increase in fluorescence emission intensity from NBD-PE (Cuevas Arenas et al., 2017; Grethen et al., 2018; Danielczak and Keller, 2018). Following this approach, we observed faster lipid transfer with increasing concentrations of Mg^{2+} (Fig. 3a) or Ca^{2+} (Fig. 3b) at a given lipid concentration. Fits to the experimental data according to Eq. (1) unveiled a monotonic increase in the observed rate constant, k_{obs}, from 0.02 s^{-1} in the absence of divalent cations to 0.30 s^{-1} and 0.40 s^{-1} in the presence of 10 mM Mg^{2+} and 7.5 mM Ca^{2+}, respectively. At the millimolar lipid concentrations used here, the dominant contribution to lipid exchange among DIBMALPs comes from binary collisions between two nanodiscs (Danielczak and Keller, 2018). Consequently, the second-order rate constant characterising the kinetics of lipid exchange through binary collisions can, to a very good degree, be approximated as $k_{bi} \approx k_{obs}/c_L$, with $c_L = 5$ mM being the lipid concentration in unlabelled nanodiscs. Accordingly, k_{bi} increased from 3.1 $M^{-1}s^{-1}$ without divalent cations to 59 $M^{-1}s^{-1}$ and 79 $M^{-1}s^{-1}$ at 10 mM Mg^{2+} and 7.5 mM Ca^{2+}, respectively (Fig. 3c). Thus, k_{bi} increased by factors of ~20 and ~25 for Mg^{2+} and Ca^{2+}, respectively. For comparison, raising the concentration of NaCl from 200 mM to 400 mM results in an acceleration by a factor of ~7 only (Danielczak and Keller, 2018).

The drastic acceleration afforded by low concentrations of divalent cations is impossible to rationalise by invoking only Coulombic screening resulting from an increase in ionic strength, as explained in the following. We have previously shown (Danielczak and Keller, 2018) that the dependence of k_{bi} on ionic strength, *I*, can be modelled by using an extended form of the Debye–Hückel equation (Bergethon, 2010) to describe the primary kinetic salt effect (Brønsted, 1922). As addition of 10 mM of a fully dissociating chloride salt of a divalent cation to 200 mM NaCl raises *I* only slightly from 200 mM to 230 mM, Eq. (2) predicts an increase in k_{bi} from 3.1 $M^{-1}s^{-1}$ to 4.2 $M^{-1}s^{-1}$ only, irrespective of the chemical nature of the divalent cation (Fig. 3c, grey dashed line). Our findings that $CaCl_2$ had a stronger influence than $MgCl_2$ and that both alkaline earth metal salts had a much stronger effect than expected for simple Coulombic screening therefore suggest that Mg^{2+} and Ca^{2+} ions associate with DIBMALPs in a specific manner.

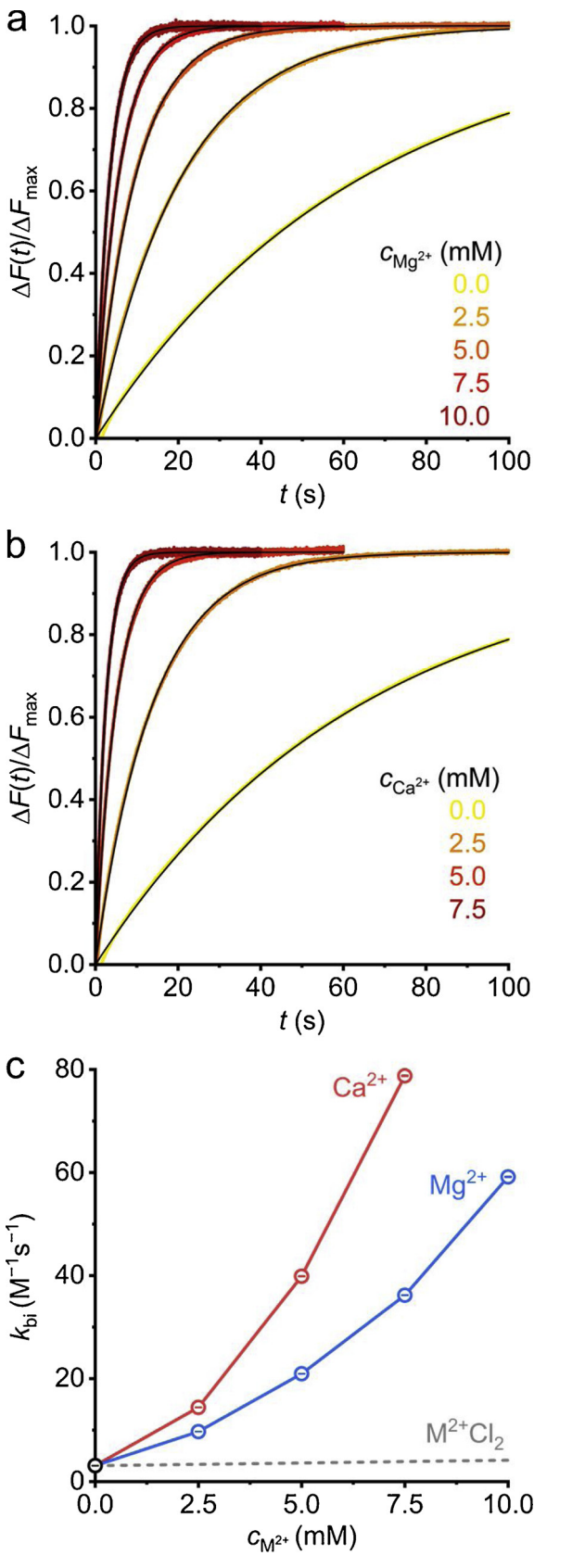

(caption on next page)

Counterion association with polyelectrolytes follows complex, linked equilibria; in particular, divalent counterions can associate with

Fig. 3. Lipid transfer among fluorescently labelled and unlabelled DIBMALPs at 30 °C and increasing c_M^{2+} as monitored by TR-FRET. (a,b) Normalised NBD-PE fluorescence intensity, $\Delta F(t)/\Delta F_{max}$, versus time, t, upon mixing labelled and unlabelled DIBMALPs at final lipid concentrations of 2.5 mM and 5 mM, respectively, in the presence of various concentrations of (a) Mg^{2+} or (b) Ca^{2+}. Shown are experimental data (coloured dots) and corresponding fits (black lines) based on Eq. (1). (c) Second-order rate constants of collisional lipid transfer, k_{bi}, derived from experimental traces in panels a and b (solid lines) or predicted by Eq. (2) for simple Coulombic screening (grey dashed line) as functions of c_M^{2+}. Data points are from fits (circles) as derived from Eq. (1). Error bars (within circles) represent 99% confidence intervals.

the carboxylate groups in copolymers containing maleic acid in different stoichiometries and, furthermore, compete with protons (Bretti et al., 2005). Therefore, we refrained from a more detailed, quantitative analysis, which additionally would have to account for differences in counterion association between free and nanodisc-bound polymer chains and also consider interactions with lipid headgroups (Lis et al., 1981; Alsop et al., 2016). Notwithstanding, it is reassuring to find that the effects of divalent cations on the kinetics of DIBMA-mediated membrane solubilisation (Fig. 1), on the equilibrium efficiency of the same process (Fig. 2), and on the kinetics of collisional lipid exchange among DIBMALPs (Fig. 3) all manifest in the low millimolar Mg^{2+} or Ca^{2+} concentration range, as the dissociation constants of both ions from maleic acid have been reported to fall into this range (Kläning and Østerby, 1976).

3.3. Nanodisc morphology and bilayer architecture

Because both Mg^{2+} and Ca^{2+} exert drastic effects on lipid solubilisation and exchange dynamics, we sought to confirm that the nanoparticles formed in the presence of these divalent cations retained a nanodisc morphology and a lipid-bilayer architecture rather than being mixed micelles. Both in the presence of Mg^{2+} (Fig. 4a) or Ca^{2+} (Fig. 4b), TEM clearly corroborated the existence of nanodiscs very similar to those observed previously in the absence of divalent cations (Oluwole et al., 2017a). We then employed DSC to probe the thermotropic gel-to-fluid transition of DMPC, which is characteristic of a bilayer architecture but absent from purely fluid-phase micellar assemblies. All DIBMALP samples gave rise to relatively broad transitions (Fig. 4c), which are typical and indicative of nanosized lipid-bilayer patches (Orwick et al., 2012; Grethen et al., 2017; Oluwole et al., 2017a). Interestingly, the presence of 10 mM Mg^{2+} or 7.5 mM Ca^{2+} reduced the main transition temperature, T_m, from ~24 °C to ~22 °C. Since an increase in the DIBMA/DMPC ratio similarly results in a decrease in T_m (Oluwole et al., 2017a), the present observations are in accordance with the above conclusion that divalent cations render DIBMA more efficient in associating with and solubilising phospholipids.

3.4. Extraction of membrane proteins from cellular membranes

Finally, we wondered whether the strong effects of Mg^{2+} and Ca^{2+} on the formation and the dynamics of DIBMALPs would manifest also in the extraction of proteins from cellular membranes. Hence, we quantified time-dependent protein-extraction yields from *E. coli* membranes both in the absence and in the presence of divalent cations. Specifically, membrane pellets were exposed for 0.2–23 h to 3.0 mM (i.e., 2.5% (*w/v*)) DIBMA without or with either 10 mM Mg^{2+} or 7.5 mM Ca^{2+}, then separated from unsolubilised material by ultracentrifugation, and finally subjected to SDS-PAGE (Fig. 5a). The resulting protein-extraction yields were quantified by densitometry (Fig. 5b). Under all conditions, protein yields after 12 min of incubation amounted to > 40% relative to the value after 23 h in the absence of divalent cations. At longer incubation times, the presence of Mg^{2+} and, to an even greater extent, Ca^{2+} resulted in a steeper increase in protein yield as compared with

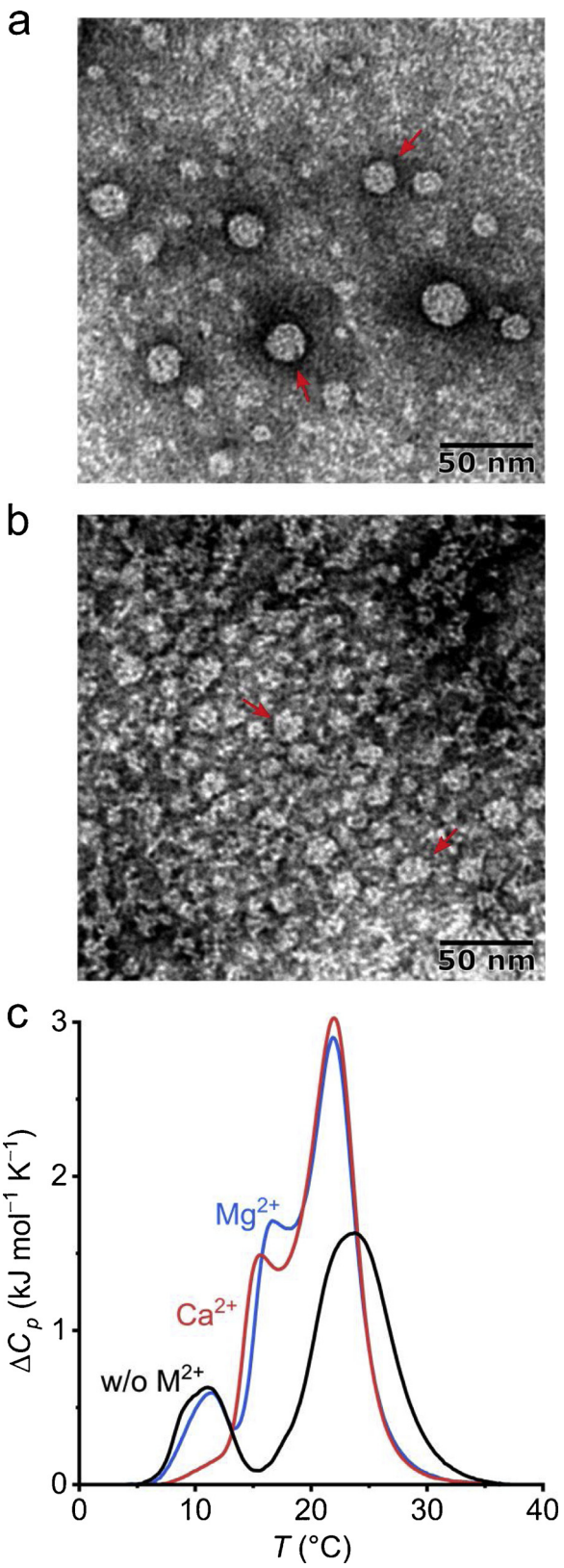

Fig. 4. Influence of divalent cations on nanodisc morphology and thermotropic phase behaviour. (a,b) TEM images of DIBMALPs at c_{DIBMA}/c_{POPC} = 0.5 in the presence of (a) 10 mM Mg^{2+} or (b) 10 mM Ca^{2+}. Red arrows indicate nanodiscs in face-on orientation. (c) DSC thermograms showing excess molar isobaric heat capacities, ΔC_p, as functions of temperature, T, for 5 mM DMPC and 0.5 mM DIBMA without divalent cations or with either 10 mM Mg^{2+} or 7.5 mM Ca^{2+}.

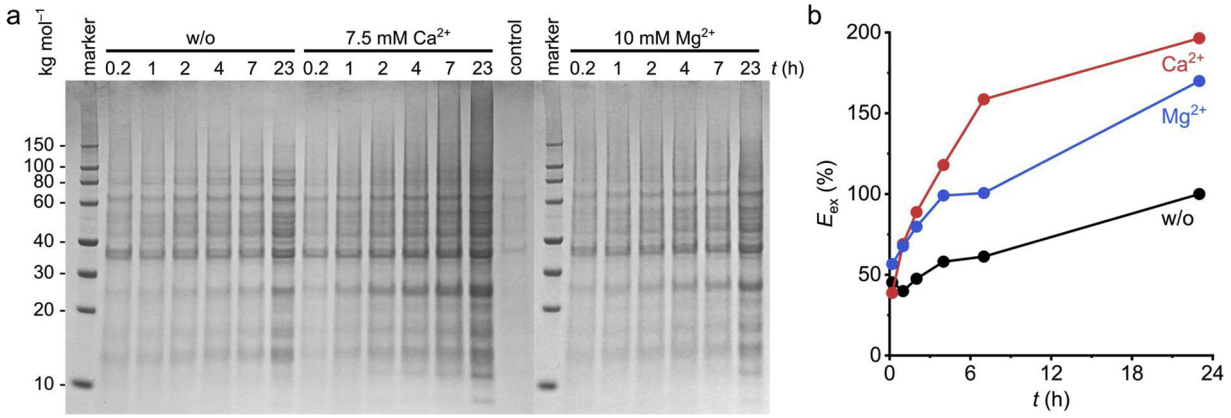

Fig. 5. Kinetics and yields of membrane-protein extraction from *E. coli* BL21(DE3) membranes by 3.0 mM (i.e., 2.5% (*w/v*)) DIBMA in the absence and presence of divalent cations. (a) SDS-PAGE of solubilised membrane-protein fractions after removal of cell debris, intrinsically soluble proteins, and unsolubilised material by serial ultracentrifugation. Samples were taken after 0.2, 1, 2, 4, 7, and 23 h of incubation at 25 °C. A control without DIBMA was incubated for 23 h at the same temperature. (b) Extraction efficiencies, E_{ex}, as functions of incubation time, *t*, as derived from data in panel a. 100% corresponds to the maximal yield after 23 h in the absence of divalent cations.

extraction trials performed without divalent cations. After 23 h of incubation, 10 mM Mg^{2+} and 7.5 mM Ca^{2+} afforded improvements in protein-extraction yield by factors of 1.6 and 1.9, respectively.

Strong Coulombic repulsion has to be overcome for polyanionic DIBMA in order to adsorb to *E. coli* membranes, which are also highly anionic (Raetz and Dowhan, 1990). Similar to the case of collisional lipid exchange among nanodiscs, simple Coulombic screening as brought about by elevated concentrations of monovalent ions in the aqueous solution should have, at best, a moderate effect on these repulsive interactions. Indeed, we have previously observed (Grethen et al., 2017) that increasing the NaCl concentration from 200 mM to 500 mM does not significantly affect protein extraction under otherwise identical conditions. In stark contrast with this, counterion association as commonly observed for multivalent counterions—and, specifically, for Mg^{2+} and Ca^{2+} binding to DIBMA—can effectively neutralise a considerable fraction of the ionisable groups on the polymer. Moreover, divalent cations associate particularly with anionic lipid headgroups (Melcrová et al., 2016), thus further attenuating Coulombic repulsion.

4. Conclusions

Low millimolar concentrations of Mg^{2+} or Ca^{2+} have major effects on the formation and dynamics of DIBMALPs and on the extraction of membrane proteins from cellular membranes with the aid of DIBMA. In particular, these divalent cations

- accelerate DIBMA-mediated solubilisation of model membranes,
- increase the equilibrium efficiency of membrane solubilisation,
- speed up lipid transfer among nanodiscs bounded by DIBMA, but
- retain lipid-bilayer architecture and nanodisc morphology, and
- improve protein-extraction yields from *E. coli* membranes.

These strong effects cannot be explained by simple Coulombic screening but are due to partial neutralisation of DIBMA's carboxylate groups by association of Mg^{2+} and Ca^{2+} ions. The observation that SMA copolymers are less tolerant than DIBMA to divalent cations can then be explained by the lower density of carboxylate groups found in the former group of polymers. As a corollary, lower Mg^{2+} and Ca^{2+} concentrations will suffice to increase the effective hydrophobicity of SMA copolymers beyond the point at which they remain soluble in aqueous solution. With regard to applications, the present findings suggest that low, physiologically compatible concentrations of multivalent cations should help improve the efficiency of membrane-protein extraction by DIBMA and, possibly, other amphiphilic copolymers.

Conflicts of interest

None.

Acknowledgements

We thank Anne Grethen and Karin Gries (both TUK) for helpful discussions and for kindly providing *E. coli* cell pellets, respectively. This work was supported by the Carl Zeiss Foundation through the Centre for Lipidomics (CZSLip) and the Deutsche Forschungsgemeinschaft (DFG) through International Research Training Group (IRTG) 1830.

References

Alsop, R.J., Maria Schober, R., Rheinstädter, M.C., 2016. Swelling of phospholipid membranes by divalent metal ions depends on the location of the ions in the bilayers. Soft Matter 12, 6737–6748. https://doi.org/10.1039/c6sm00695g.

Barniol-Xicota, M., Verhelst, S.H.L., 2018. Stable and functional rhomboid proteases in lipid nanodiscs by using diisobutylene/maleic acid copolymers. J. Am. Chem. Soc. 140, 14557–14561. https://doi.org/10.1021/jacs.8b08441.

Bergethon, P.R., 2010. The Physical Basis of Biochemistry: The Foundations of Molecular Biophysics, 2nd. ed. Springer, New York.

Bersch, B., Dörr, J.M., Hessel, A., Killian, J.A., Schanda, P., 2017. Proton-detected solid-state NMR spectroscopy of a zinc diffusion facilitator protein in native nanodiscs. Angew. Chem. Int. Ed. 56, 2508–2512. https://doi.org/10.1002/anie.201610441.

Bretti, C., Crea, F., Rey-Castro, C., Sammartano, S., 2005. Interaction of acrylic-maleic copolymers with H^+, Na^+, Mg^{2+} and Ca^{2+}: thermodynamic parameters and their dependence on medium. React. Funct. Polym. 65, 329–342. https://doi.org/10.1016/j.reactfunctpolym.2005.07.005.

Broecker, J., Eger, B.T., Ernst, O.P., 2017. Crystallogenesis of membrane proteins mediated by polymer-bounded lipid nanodiscs. Structure 25, 384–392. https://doi.org/10.1016/j.str.2016.12.004.

Brønsted, J.N., 1922. Zur Theorie der chemischen Reaktionsgeschwindigkeit. Z. Phys. Chem. 102, 169–207.

Cuevas Arenas, R., Danielczak, B., Martel, A., Porcar, L., Breyton, C., Ebel, C., Keller, S., 2017. Fast collisional lipid transfer among polymer-bounded nanodiscs. Sci. Rep. 7, 45875. https://doi.org/10.1038/srep45875.

Damian, M., Pons, V., Renault, P., M'Kadmi, C., Delort, B., Hartmann, L., Kaya, A.I., Louet, M., Gagne, D., Haj, Ben, Salah, K., Denoyelle, S., Ferry, G., Boutin, J.A., Wagner, R., Fehrentz, J.A., Martinez, J., Marie, J., Floquet, N., Galès, C., Mary, S., Hamm, H.E., Banères, J.L., 2018. GHSR-D2R heteromerization modulates dopamine signaling through an effect on G protein conformation. Proc. Natl. Acad. Sci. U. S. A. 115, 4501–4506. https://doi.org/10.1073/pnas.1712725115.

Danielczak, B., Keller, S., 2018. Collisional lipid exchange among DIBMA-encapsulated nanodiscs (DIBMALPs). Eur. Pol. J. 109, 206–213. https://doi.org/10.1016/j.eurpolymj.2018.09.043.

Dörr, J.M., 2017. Membrane Solubilization by Styrene-maleic Acid Copolymers: Towards New Applications in Membrane Protein Research. PhD Thesis. Utrecht. .

Dörr, J.M., Koorengevel, M.C., Schäfer, M., Prokofyev, A.V., Scheidelaar, S., van der Cruijsen, E.A., Dafforn, T.R., Baldus, M., Killian, J.A., 2014. Detergent-free isolation, characterization, and functional reconstitution of a tetrameric K+ channel: the power of native nanodiscs. Proc. Natl. Acad. Sci. U. S. A. 111 (52), 18607–18612.

https://doi.org/10.1073/pnas.1416205112.
Ederth, C., 2000. Forces between carboxylic acid surfaces in divalent electrolyte solutions. J. Colloid Interface Sci. 229, 123–128. https://doi.org/10.1006/jcis.2000.6961.
Grethen, A., Oluwole, A.O., Danielczak, B., Vargas, C., Keller, S., 2017. Thermodynamics of nanodisc formation mediated by styrene/maleic acid (2:1) copolymer. Sci. Rep. 7, 11517. https://doi.org/10.1038/s41598-017-11616-z.
Grethen, A., Glueck, D., Keller, S., 2018. Role of Coulombic repulsion in collisional lipid transfer among SMA(2:1)-bounded nanodiscs. J. Membr. Biol. https://doi.org/10.1007/s00232-018-0024-0.
Gulati, S., Jamshad, M., Knowles, T.J., Morrison, K.A., Downing, R., Cant, N., Collins, R., Koenderink, J.B., Ford, R.C., Overduin, M., Kerr, I.D., Dafforn, T.R., Rothnie, A.J., 2014. Detergent-free purification of ABC (ATP-binding-cassette) transporters. Biochem. J. 461, 269–278. https://doi.org/10.1042/BJ20131477.
Hall, S.C.L., Tognoloni, C., Charlton, J., Bragginton, É.C., Rothnie, A.J., Sridhar, P., Wheatley, M., Knowles, T.J., Arnold, T., Edler, K.J., Dafforn, T.R., 2018. An acid-compatible co-polymer for the solubilization of membranes and proteins into lipid bilayer-containing nanoparticles. Nanoscale 10, 10609–10619. https://doi.org/10.1039/c8nr01322e.
Hassan, P.A., Rana, S., Verma, G., 2015. Making sense of Brownian motion: colloid characterization by dynamic light scattering. Langmuir 31, 3–12. https://doi.org/10.1021/la501789z.
Jamshad, M., Charlton, J., Lin, Y., Routledge, S.J., Bawa, Z., Knowles, T.J., Overduin, M., Dekker, N., Dafforn, T.R., Bill, R.M., Poyner, D.R., Wheatley, M., 2015. G-protein coupled receptor solubilization and purification for biophysical analysis and functional studies, in the total absence of detergent. Biosci. Rep. 35. https://doi.org/10.1042/BSR20140171.
Kemmer, G., Keller, S., 2010. Nonlinear least-squares data fitting in Excel spreadsheets. Nat. Prot. 5, 267–281. https://doi.org/10.1038/nprot.2009.182.
Kläning, U.K., Østerby, O., 1976. Hydration and ion pairing of maleinates, malonates, and substituted malonates in aqueous solution. J. Chem. Soc. Faraday Trans. 1 (72), 513. https://doi.org/10.1039/F19767200513.
Knowles, T.J., Finka, R., Smith, C., Lin, Y., Dafforn, T.R., Overduin, M., 2009. Membrane proteins solubilized intact in lipid containing nanoparticles bounded by styrene maleic acid copolymer. J. Am. Chem. Soc. 131, 7484–7485. https://doi.org/10.1021/ja810046q.
Koppel, D.E., 1972. Analysis of macromolecular polydispersity in intensity correlation spectroscopy. The method of cumulants. J. Chem. Phys. 57, 4814–4820. https://doi.org/10.1063/1.1678153.
Lee, S.C., Knowles, T.J., Postis, V.L.G., Jamshad, M., Parslow, R.A., Lin, Y., Goldman, A., Sridhar, P., Overduin, M., Muench, S.P., Dafforn, T.R., 2016. A method for detergent-free isolation of membrane proteins in their local lipid environment. Nat. Prot. 11, 1149–1162. https://doi.org/10.1038/nprot.2016.070.
Lis, L.J., Lis, W.T., Parsegian, V.A., Rand, R.P., 1981. Adsorption of divalent cations to a variety of phosphatidylcholine bilayers. Biochemistry 20, 1771–1777. https://doi.org/10.1021/bi00510a010.
Logez, C., Damian, M., Legros, C., Dupré, C., Guéry, M., Mary, S., Wagner, R., M'Kadmi, C., Nosjean, O., Fould, B., Marie, J., Fehrentz, J., Martinez, J., Ferry, G., Boutin, J.A., Banères, J., 2016. Detergent-free isolation of functional G protein-coupled receptors into nanometric lipid particles. Biochemistry 55, 38–48. https://doi.org/10.1021/acs.biochem.5b01040.
Melcrová, A., Pokorna, S., Pullanchery, S., Kohagen, M., Jurkiewicz, P., Hof, M., Jungwirth, P., Cremer, P.S., Cwiklik, L., 2016. The complex nature of calcium cation interactions with phospholipid bilayers. Sci. Rep. 6, 38035. https://doi.org/10.1038/srep38035.
Moelwyn-Hughes, E.A., 1963. Ionic association. Z. Naturforsch. A 18. https://doi.org/10.1515/zna-1963-0216.
Nichols, J.W., Pagano, R.E., 1983. Resonance energy transfer assay of protein-mediated lipid transfer between vesicles. J. Biol. Chem. 258, 5368–5371.
Oluwole, A.O., Danielczak, B., Meister, A., Babalola, J.O., Vargas, C., Keller, S., 2017a. Solubilization of membrane proteins into functional lipid-bilayer nanodiscs using a diisobutylene/maleic acid copolymer. Angew. Chem. Int. Ed. 56, 1919–1924. https://doi.org/10.1002/anie.201610778.
Oluwole, A.O., Klingler, J., Danielczak, B., Babalola, J.O., Vargas, C., Pabst, G., Keller, S., 2017b. Formation of lipid-bilayer nanodiscs by diisobutylene/maleic acid (DIBMA) copolymer. Langmuir 33, 14378–14388. https://doi.org/10.1021/acs.langmuir.7b03742.
Orwick, M.C., Judge, P.J., Procek, J., Lindholm, L., Graziadei, A., Engel, A., Gröbner, G., Watts, A., 2012. Detergent-free formation and physicochemical characterization of nanosized lipid-polymer complexes: lipodisq. Angew. Chem. Int. Ed. 51, 4653–4657.
Orwick-Rydmark, M., Lovett, J.E., Graziadei, A., Lindholm, L., Hicks, M.R., Watts, A., 2012. Detergent-free incorporation of a seven-transmembrane receptor protein into nanosized bilayer Lipodisq particles for functional and biophysical studies. Nano Lett. 12, 4687–4692. https://doi.org/10.1021/nl3020395.
Parmar, M., Rawson, S., Scarff, C.A., Goldman, A., Dafforn, T.R., Muench, S.P., Postis, V.L.G., 2017. Using a SMALP platform to determine a sub-nm single particle cryo-EM membrane protein structure. Biochim. Biophys. Acta 1860, 378–383. https://doi.org/10.1016/j.bbamem.2017.10.005.
Raetz, C.R., Dowhan, W., 1990. Biosynthesis and function of phospholipids in *Escherichia coli*. J. Biol. Chem. 265, 1235–1238.
Scheidelaar, S., Koorengevel, M.C., Pardo, J.D., Meeldijk, J.D., Breukink, E., Killian, J.A., 2015. Molecular model for the solubilization of membranes into nanodisks by styrene maleic acid copolymers. Biophys. J. 108, 279–290. https://doi.org/10.1016/j.bpj.2014.11.3464.
Scheidelaar, S., Koorengevel, M.C., van Walree, C.A., Dominguez, J.J., Dörr, J.M., Killian, J.A., 2016. Effect of polymer composition and pH on membrane solubilization by styrene-maleic acid copolymers. Biophys. J. 111, 1974–1986. https://doi.org/10.1016/j.bpj.2016.09.025.
Schneider, C.A., Rasband, W.S., Eliceiri, K.W., 2012. NIH image to ImageJ: 25 years of image analysis. Nat. Methods 9, 671–675.
Sun, C., Benlekbir, S., Venkatakrishnan, P., Wang, Y., Hong, S., Hosler, J., Tajkhorshid, E., Rubinstein, J.L., Gennis, R.B., 2018. Structure of the alternative complex III in a supercomplex with cytochrome oxidase. Nature 557, 123–126. https://doi.org/10.1038/s41586-018-0061-y.
Tonge, S.R., Tighe, B.J., 2001. Responsive hydrophobically associating polymers: a review of structure and properties. Adv. Drug Deliv. Rev. 53, 109–122.
Wessel, D., Flügge, U.I., 1984. A method for the quantitative recovery of protein in dilute solution in the presence of detergents and lipids. Anal. Biochem. 138, 141–143. https://doi.org/10.1016/0003-2697(84)90782-6.